EEET ECOLOGICAL ENGINEERING & ENVIRONMENTAL TECHNOLOGY

Ecological Engineering & Environmental Technology, 2026, 27(9), 182–196
https://doi.org/10.12912/27197050/226169
ISSN 2719–7050, License CC-BY 4.0

Received: 2026.07.09
Accepted: 2026.07.31
Published: 2026.08.15

GIS-based analytic hierarchy process for flood susceptibility zoning in the coastal lowland: A case study of Saidia City, northeast of Morocco

Adil Jouamaa[1*], Mimoun Chourak[1], Zerhoudi Imad[2], Chaaraoui Aboubakr[3], Maelaynayn El Baida[1]

[1] National School of Applied Sciences of Oujda, Mohammed First University, Oujda, Morocco
[2] Faculty of Sciences, Mohammed First University, Oujda, Morocco
[3] Agency for the Development of the Marchica Lagoon Site, 62000 Nador, Morocco
* Corresponding author's e-mail: adil.jouamaa@ump.ac.ma

ABSTRACT

The city of Saidia is a coastal Mediterranean urban lowland characterized by concentrated population, tourism infrastructure, and seasonal watercourses. This combination makes the city exposed to inundation. This study maps and assesses pluvial and fluvial flood susceptibility across the coastal area of the city of Saidia using the analytic hierarchy process (AHP) and geographic information system (GIS). Seven conditioning factors were selected and processed as raster layers including elevation, slope, topographic wetness index (TWI), normalized difference vegetation index (NDVI), distance to rivers, distance to roads, and drainage density. The pairwise comparison matrix obtained through expert judgments produced factor weights dominated by TWI (0.28), distance to rivers (0.20), and slope (0.18). The resulting map assigns 41.91% of the study area to the high and very high susceptibility classes. Moreover, the results suggest that the high and very high susceptibility classes are concentrated along the national road, the Moulouya river estuary, and the northern coastal plain where the urbanization occurs. The findings of this study offer valuable and instrumental planning tools for land use control and drainage prioritisation in the city of Saidia.

Keywords: flood susceptibility, analytic hierarchy process, geographic information system, multi-criteria decision analysis, coastal lowland, Saidia.

INTRODUCTION

Flooding is the most damaging natural hazard across the Middle East and North Africa (MENA), a region where arid and semi-arid rivers alternate long dry spells with sudden torrential discharges (Kantoush et al., 2022; Loudyi and Kantoush, 2020). Morocco is no exception: extreme precipitation along its Mediterranean margin is projected to intensify under climate change (Tramblay et al., 2012), and continental-scale analyses of African catchments show that flooding across the northern part of the continent is driven mainly by prolonged, excess rainfall rather than by soil-moisture seasonality (Tramblay et al., 2021, 2022). The rapid expansion of coastal cities has meanwhile multiplied the assets exposed to inundation, a trend well documented along the Moroccan shoreline, where resort and marina developments have encroached on land that was once naturally floodable (Aitali et al., 2020; Snoussi et al., 2008). Continent-wide analyses confirm that this trajectory is not confined to North Africa: flooding across West Africa is likewise intensifying as rainfall variability increases over rapidly expanding floodplain settlements (Tramblay et al., 2021, 2022), indicating that the exposure dynamics documented here belong to a broader African pattern. Comparable evidence from West Africa links increasing climate variability and shifting precipitation regimes to growing exposure to climate stress in floodplain settlements of the Niger Delta (Odiana et al., 2026).

A wide methodological spectrum is available for anticipating where floodwater will concentrate, the first step of any risk-reduction strategy, ranging from physically based hydraulic simulation to statistical and data-driven mapping (Maranzoni et al., 2023; Teng et al., 2017). Hydrodynamic models produce depth and velocity fields, but they require design discharges, fine terrain models, and calibration data that most Moroccan municipalities simply do not have, and their mapped domain is limited to reaches downstream of a hydrological station (Bouchikhi et al., 2025). Machine-learning classifiers relax some of these requirements: they have already produced high-resolution hazard maps for the nearby city of Zaio (El Baida et al., 2024a, 2024c) and for various urban settings elsewhere (Eini et al., 2020; Norallahi and Kaboli, 2021; Shikhteymour et al., 2023), while deep-learning surrogates now reproduce hydrodynamic outputs at a fraction of the computational cost (El Baida et al., 2025b). All of these approaches, however, depend on inventories of observed flood locations, and the scarcity or unreliability of such inventories in African urban settings is well documented (El Baida et al., 2024b; Mudashiru et al., 2021b).

Throughout this study, the terms are used in their standard sense: flood susceptibility is the intrinsic, magnitude-independent tendency of an area to be inundated given its physical setting; flood hazard adds the probability and intensity (depth, velocity, frequency) of flooding; and flood risk combines hazard with the exposure and vulnerability of the elements at stake. The model developed here maps susceptibility, not hazard or risk.

Multi-criteria decision analysis takes a different route: it substitutes structured expert judgment for missing observations and can therefore be applied wherever the conditioning factors can be mapped (Mudashiru et al., 2021a). Within this family, the analytic hierarchy process introduced by Saaty (1977) remains the most widely used scheme for flood zonation, since it converts qualitative pairwise comparisons into ratio-scale weights while offering a built-in check on the coherence of the judgments (Dung et al., 2022). It has since been applied to data-scarce basins in India (Ramkar and Yadav, 2021), combined with fuzzy and statistical methods (Akay, 2021), extended to tectonically active Mediterranean catchments (Bathrellos et al., 2016; Skilodimou et al., 2025), paired with frequency-ratio models in Pakistan, Japan, and Ghana (Ashfaq et al., 2025; Elsadek et al., 2024; Frimpong et al., 2026), and coupled with machine learning (Deroliya et al., 2022).

Morocco itself has contributed a dense cluster of case studies to this literature. In the Dades wadi watershed of the Central High Atlas, an AHP–GIS assessment reached an area under the curve of 85% (Aichi et al., 2024), while in the semi-arid Seyad basin a flood hazard index classified 31.12% of the territory as highly susceptible (Echogdali et al., 2022). Closer to the present study area, along the lower Moulouya corridor, AHP zoning has been confronted with two-dimensional hydraulic modelling at Driouch (El Hadri et al., 2025), validated against reported flood locations at greater Berkane, where it retained 80.74% of events within its high and very high classes (Zerhoudi et al., 2026), and combined with hydrodynamic simulation at Oued Merzeg near Casablanca to reveal settlements lying outside the officially protected zones (Bouchikhi et al., 2025). Together, these results suggest that a carefully weighted multi-criteria scheme can deliver planning-grade susceptibility maps precisely where discharge records and flood inventories are lacking.

The eastern Mediterranean coast of Morocco has been identified as one of the national sectors most vulnerable to flooding and sea-level rise (Snoussi et al., 2008), and the Saidia resort complex in particular has been singled out as a case of construction advancing onto flood-prone ground (Aitali et al., 2020). This study addresses that gap through four objectives: (i) assembling a consistent seven-factor geodatabase over the Saidia coastal area; (ii) deriving AHP weights from a pairwise comparison matrix anchored in the regional literature and verifying their internal consistency; (iii) producing a five-class pluvial and fluvial susceptibility map through weighted overlay and natural-breaks classification; and (iv) comparing the resulting zoning with the recent body of Moroccan case studies. Nature-based orientations for the most exposed sectors are discussed as well, in line with the mitigation pathways already evaluated for the region under climate-change forcing (El Baida et al., 2025a). In this framing, the contribution is a regional-scale planning framework for flood-susceptibility assessment in a data-scarce Moroccan coastal environment, supported by cross-comparison with independent hydraulic studies, rather than a methodological advance in AHP itself.

STUDY AREA

Geographic setting

The study area covers approximately 71 km² at the eastern end of the Trifa plain, in Berkane province (Oriental Region, northeastern Morocco), and includes the seaside town of Saidia along with its agricultural and peri-urban surroundings. The Trifa plain is bounded by the Ouled Mansour hills and the Mediterranean shoreline to the north, the Beni Snassen mountains to the south, the Moulouya River and its tributary Cherraa to the west, and Oued Kiss, which marks the Algerian border, to the east (Fetouani et al., 2008). Within the modelled grid, elevation drops from about 181 m on the first southern foothills to sea level along the shore, and much of the coastal plain sits below 20 m. Slopes exceed 30° only on the southern reliefs and stay below a few degrees over most of the plain, a configuration that favours the ponding of surface water once it leaves the incised upstream channels (Figure 1).

Geology and geomorphology

The Trifa plain constitutes a basin set within the north-eastern Moroccan foreland that is bounded to the south by the Beni Snassen massif and by Kebdana mountains in the north-west; the main faults governing this structural arrangement have been delineated through gravimetric surveying in previous studies (Chennouf et al., 2007). The basin infill consists of Mio-Pliocene and Quaternary continental deposits (alluvial silts, red clays, lacustrine limestones and conglomerates) resting upon folded Jurassic carbonate series that crop out in the bordering reliefs (El Idrysy and De Smedt, 2006; Sardinha et al., 2012). The marly and clayey piedmont formations restrict infiltration and promote surface runoff, such that precipitation falling on the Beni Snassen slopes is transmitted rapidly onto the plain; investigations into salinisation processes corroborate the closed, low-gradient character of the northern sub-basins, where drainage remains notably diminished (Boughriba et al., 2006). The coastline is configured as a sandy, dune-backed accretionary system historically nourished by Moulouya-derived alluvium. Dam construction within the catchment has reduced fluvial sediment delivery by approximately half, and the consequent erosional readjustment of the shoreline has been further exacerbated by resort and marina development undertaken over the past two decades (Aitali et al., 2020; Snoussi et al., 2002) (Figure 2).

Climate and hydrology

The study area is characterized by a semi-arid Mediterranean climate, which consists of

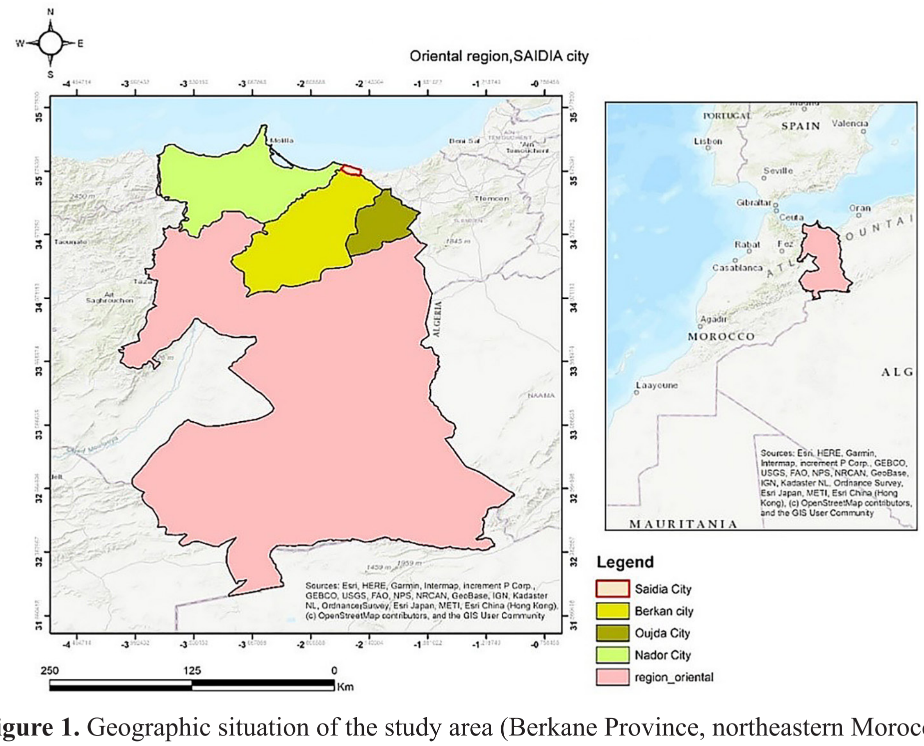

Figure 1. Geographic situation of the study area (Berkane Province, northeastern Morocco)

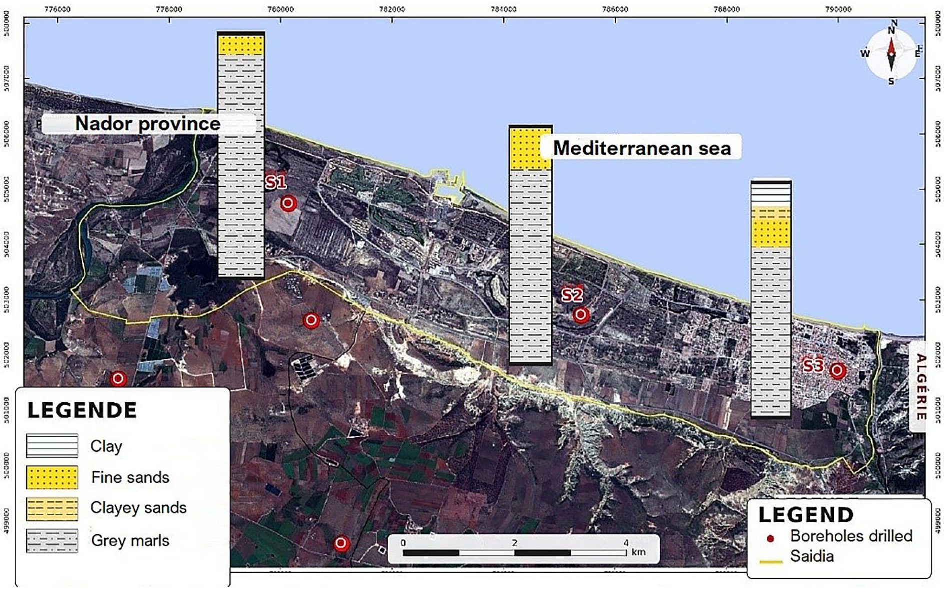

Figure 2. Geomorphology of the study area

dry summers and a modest rainfall total concentrated between autumn and early spring, and an irregular year-to-year regime in which a large share of the annual rainfall falls in limited intense events (Fetouani et al., 2008; Tramblay et al., 2012). Surface hydrography combines two systems operating at very different scales. The river of Moulouya is the longest river in Morocco, and completes its roughly 600 km course in a Mediterranean estuary in the west of Saidia; its flow is now heavily regulated by upstream dams (Snoussi et al., 2002). The plain itself is crossed by short ephemeral streams that drain the Beni Snassen mountains toward the sea; these remain dry most of the year but exhibit torrential behaviour during heavy rainfall periods. Flash floods have repeatedly impacted the neighbouring urban areas of the lower Moulouya corridor, with damaging events recorded at Berkane in 2004, 2010, 2013, 2019, and 2025 (Afif et al., 2025; Zerhoudi et al., 2026). Urbanisation along the shoreline and the main road corridors has progressively sealed the soil surface, shortening concentration times and overwhelming a stormwater network that was never sized for the current impervious extent; similar dynamics have been documented at Zaio and Driouch (El Baida et al., 2024a; El Hadri et al., 2025). Finally, the low elevation of the plain exposes its seaward fringe to marine flooding, a component already identified as critical for this stretch of the Moroccan coast under sea-level-rise scenarios (Snoussi et al., 2008) (Figure 3).

MATERIALS AND METHODS

Conditioning factors and geodatabase

Seven conditioning factors were selected for their documented influence on flood occurrence in semi-arid Mediterranean catchments and for their availability across the study area (Dung et al., 2022; El Hadri et al., 2025). All layers were prepared as GeoTIFF rasters in the WGS84 / UTM zone 30N reference system (EPSG:32630) and co-registered by bilinear resampling onto a common 8 m grid before analysis. Table 1 summarises the factors, their native characteristics, and the hydrological reasoning behind their inclusion, and Figure 4 shows the corresponding spatial layers. Geospatial workflows of this type, combining DEM derivatives and remote-sensing products within a common raster framework, are standard practice in the AHP-based flood-susceptibility literature reviewed above (Dung et al., 2022; El Hadri et al., 2025). The elevation layer was obtained from the 8 m digital elevation model provided by the Agence du Bassin Hydraulique de la Moulouya (ABHM); this DEM is natively delivered at 8 m and therefore defines the common analysis grid onto which the other layers (distance rasters, drainage density, and NDVI) were co-registered, rather than being itself resampled from a coarser source. The NDVI layer was derived from Landsat 8/9 OLI imagery acquired on 25 September 2023, at its native 30

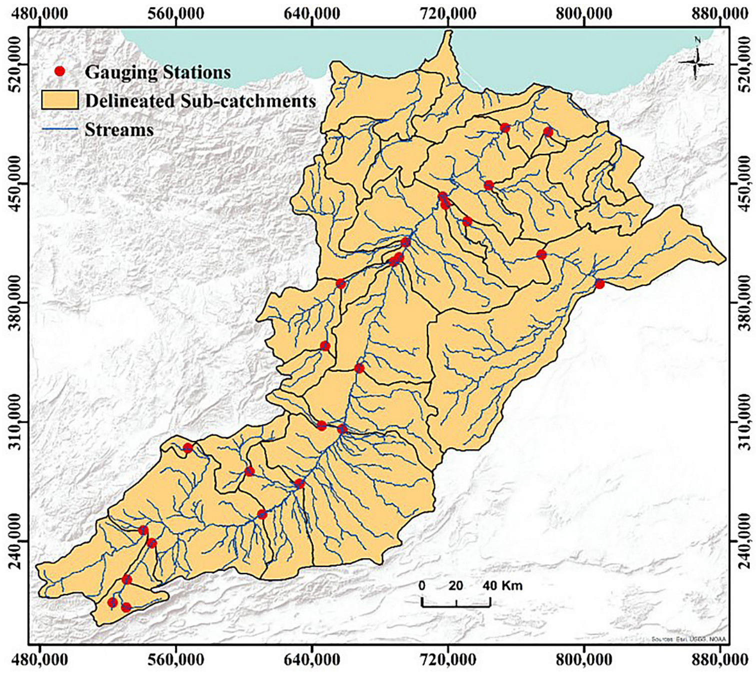

Figure 3. Moulouya basin with delineated sub-catchments

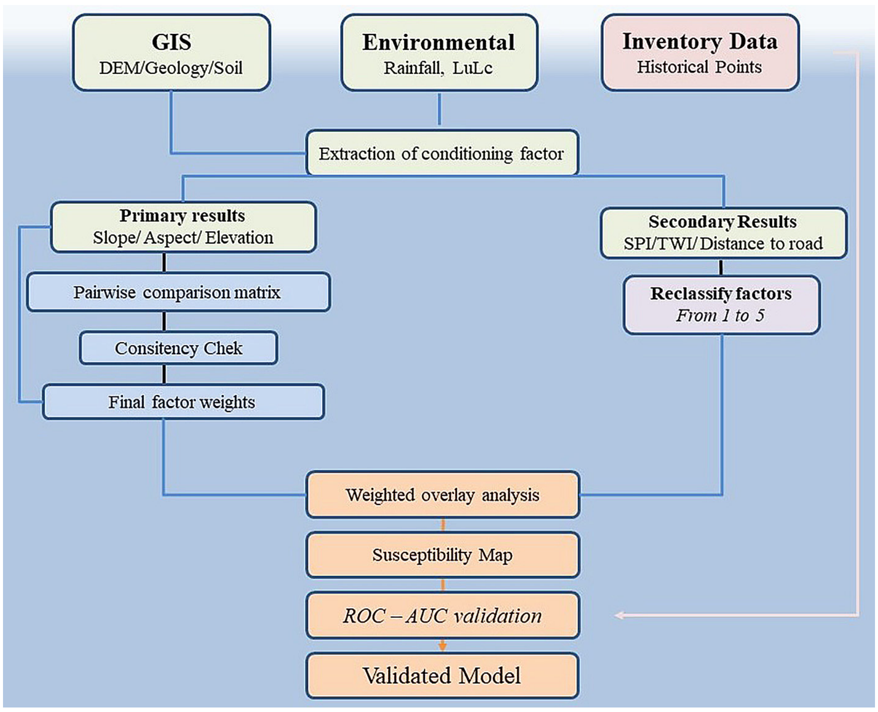

Figure 4. Methodology flowchart

m resolution, and resampled bilinearly onto the common 8 m grid; vegetation cover varies far more smoothly in space than terrain attributes, so this oversampling introduces no artificial spatial detail, and the 3.3% weight of NDVI bounds the influence of any residual resampling artefact on the final index. Comparable remote-sensing and terrain-analysis workflows have been applied to water-resource assessment, for instance in reservoir volume and 3-D topography studies (Khan and Lahori, 2024).

Table 1 – Conditioning factors used for the susceptibility assessment. The DEM (and its slope, TWI, distance-to-river, and drainage-density

derivatives) and the road network were provided by the Agence du Bassin Hydraulique de la Moulouya (ABHM); the river/wadi network was extracted automatically from the DEM by flow-accumulation analysis; NDVI was derived from Landsat 8/9 OLI imagery acquired on 25 September 2023.

Elevation and slope control two complementary processes: elevation governs the gravitational convergence of surface water toward the lowest parts of the plain (Fan et al., 2019; Gnann et al., 2025), while slope governs the velocity of overland flow, as steep gradients generally generate large peak discharges (Asfaha et al., 2015) while low and flat gradients instead promote stagnation and delay natural drainage (Armenakis and Nirupama, 2014). The topographic wetness index is calculated as TWI = ln(a / tan β), where a is the specific contributing area and β the local slope angle (Beven and Kirkby, 1979). TWI combines both effects into a single saturation-potential descriptor whose value for flood-prone land-use planning and pluvial flood detection is well established (Kelleher and McPhillips, 2020; Pourali et al., 2016). NDVI captures the moderating role of vegetation, since land cover changes are known to alter soil infiltration capacity (Sun et al., 2018). Distance to river network reflects the direct exposure of each cell to channel overflow. The distance-to-rivers layer was computed from the complete mapped channel network, including ephemeral channels: in the semi-arid regime of the study area, the ephemeral wadis draining the Beni Snassen piedmont are the dominant flood conveyors, and restricting the network to perennial reaches, essentially the terminal Moulouya, would remove the very channels responsible for most recorded flood damage in the region (Zerhoudi et al., 2026), a factor consistently used in both data-driven and multi-criteria studies (Hasanuzzaman et al., 2023; Özay and Orhan, 2023). Distance to roads captures the contribution of sealed linear infrastructure to runoff production and conveyance; the relationship between roads and inundation runs in both directions, with roads amplifying flood propagation and floods, in turn, triggering road-network failure (Dong et al., 2022; Vu et al., 2024). Drainage density, finally, reflects how channelised the surface is and correlates with how quickly rainfall reaches the plain (Tehrany et al., 2015).

Analytic hierarchy process

the scale (Saaty, 1977). The comparison matrix used here (Table 2) adapts to the Saidia setting the judgment structure calibrated for the neighbouring Berkane area (Zerhoudi et al., 2026), restricted to the seven factors available over the present study area. Saidia and Berkane belong to the same lower-Moulouya corridor and share the same semi-arid flash-flood regime and low-gradient terminal-plain physiography, so the judgment structure transfers reasonably; the matrix was adapted to the locally available factors and re-checked for consistency, not copied. TWI and distance to rivers were treated as the primary flood-generation descriptors; elevation and slope received moderate dominance values, reflecting their role as topographic controls partly embedded in the TWI formulation; and distance to roads, drainage density, and NDVI were handled as secondary modulating factors.

Weights were obtained by normalising each column of the matrix to unit sum and averaging the normalised entries across each row. The coherence of the judgment set was checked through the consistency index $CI = (\lambda max - n)/(n - 1)$, where λmax is the principal eigenvalue and n = 7 the number of criteria, and the

Table 1. Conditioning factors used for the susceptibility assessment

Factor	Derived from	Cell size	Rationale
Elevation (0–181 m)	Digital elevation model	8 m	Low-lying terrain concentrates surface water
Slope (0–75.4°)	DEM derivative	8 m	Gentle gradients favour stagnation and ponding
TWI (0.8–25.3)	DEM derivative	8 m	Quantifies topographic saturation potential
NDVI (−0.21–0.51)	Satellite imagery	30 m	Vegetation cover conditions infiltration
Distance to rivers (0–708 m)	Hydrographic network (Euclidean)	8 m	Direct exposure to channel overflow
Distance to roads (0–2276 m)	Road network (Euclidean)	8 m	Sealed corridors accelerate and convey runoff
Drainage density (0–7.5 km/km²)	Hydrographic network	8 m	Channel concentration governs runoff delivery

Table 2. Pairwise comparison matrix (DR: distance to rivers; DRo: distance to roads; DD: drainage density; El: elevation; Sl: slope)

Factor	TWI	El	Sl	NDVI	DR	DRo	DD
TWI	1	2	3	7	1	3	5
Elevation	1/2	1	1	5	1	1	5
Slope	1/3	1	1	5	1	3	5
NDVI	1/7	1/5	1/5	1	1/7	1/5	1
Distance to rivers	1	1	1	7	1	3	3
Distance to roads	1/3	1	1/3	5	1/3	1	1
Drainage density	1/5	1/5	1/5	1	1/3	1	1

consistency ratio CR = CI/RI, with RI = 1.32 as the random index for a seven-by-seven matrix. The computation gives $\lambda max = 7.379$, CI = 0.063, and CR = 0.048, well below the 0.10 acceptance threshold, so the matrix was kept without revision. A low consistency ratio confirms the coherence of the judgments but not their correctness. To test robustness, a one-at-a-time sensitivity analysis was performed: the weights of the two dominant factors (TWI and distance to rivers) were perturbed by ±10% and ±20%, the weight vector renormalised, and the FS surface and class areas recomputed; the combined high and very-high area across all scenarios, indicating a robust zoning.

Reclassification and weighted overlay

Each factor layer was split into five ranks using class thresholds defined by the research team on the basis of expert judgment, drawing on the hydrological literature, the reference studies of the lower Moulouya corridor, and field knowledge of the study area. Rank 5 was assigned to the conditions most favourable to inundation: high values for TWI and drainage density, and low values for elevation, slope, NDVI, and both distance factors. The flood susceptibility index FS was subsequently calculated as the weighted linear combination $FS = \Sigma W_i X_i$, where W_i is the AHP weight of factor i and X_i its local rank. The continuous FS surface was then reclassified into five susceptibility levels, from very low to very high, using the same expert-threshold approach (El Hadri et al., 2025; Zerhoudi et al., 2026). Raster operations were carried out in a GIS environment (ArcGIS) and in Python using the rasterio library. Expert-based thresholds were preferred to purely statistical schemes such as equal intervals, quantiles, or natural breaks: the former impose arithmetic or area-equalizing cuts that ignore the hydrological meaning of each factor, whereas expert thresholds allow the class limits to be aligned with physically interpretable ranges (e.g. near-channel distance bands, low-gradient slope classes, saturation-prone TWI values) and to remain consistent with the class structure adopted in the regional reference studies, which preserves the comparability of the class proportions discussed below. It is acknowledged that expert thresholds carry a degree of subjectivity; this is examined through the sensitivity analysis presented in the following subsection.

Sensitivity analysis of the AHP weights

Since the judgment structure is transferred from a neighbouring setting, and since internal consistency (CR = 0.048) does not by itself demonstrate the correctness of the encoded assumptions, a one-at-a-time (OAT) sensitivity analysis was performed on the two dominant weights. The weights of TWI and distance to rivers were perturbed by plus or minus 10% and 20%, the six remaining weights being renormalized proportionally so that the vector retains a unit sum. For each of the eight scenarios, the susceptibility index was recomputed, reclassified into five classes using the same expert thresholds, and compared with the reference map through (i) the areal share of each class and (ii) the Spearman rank correlation of the continuous index. One-at-a-time perturbation was preferred at this stage because it isolates the influence of each dominant weight and directly answers the transferability question; a full Monte Carlo AHP, sampling the judgment matrix itself, is discussed as a perspective in the limitations section.

RESULTS AND DISCUSSION

Factor weights

The weight vector (Table 3, Figure 5) is dominated by the topographic wetness index (0.280), followed by distance to rivers (0.202), slope (0.179), and elevation (0.162); distance to roads (0.094), drainage density (0.050), and NDVI (0.033) round out the ranking. The low weight of drainage density reflects its partial collinearity with the topographic wetness index and distance-to-rivers, which already capture channel concentration, so treating it as a secondary factor avoids double-counting this signal. Saturation potential and channel proximity together account for almost half of the total weight, which fits the flash-flood regime of the area: damaging events stem from the rapid delivery of upstream runoff onto a flat plain, where topographic depressions and channel margins are the first areas to be submerged. The weight given to TWI matches studies that use the index on its own as a delineator of flood-prone ground (Pourali et al., 2016), while the low weight assigned to NDVI reflects the limited buffering capacity of sparse semi-arid vegetation against short, intense rainfall bursts.

Flood susceptibility zoning

The susceptibility map (Figure 6) shows a clear north–south gradient. The high and very high classes together cover 29.7 km², or 41.91% of the study area (Table 4, Figure 7), forming a nearly continuous belt over the northern coastal plain, where four conditions overlap: elevations close to sea level, near-zero gradients, dense convergence of the terminal drainage network, and the sealed corridors of the urban and road fabric. Within this belt, the very high class (15.65%, 11.1 km²) follows the immediate margins of the watercourses and the low-lying urbanised pockets, while the high class (26.26%, 18.6 km²) extends over the adjacent flats. The moderate class (26.01%) occupies the transitional glacis between the plain and the first slopes. The southern reliefs, with steeper gradients, greater distances from channels, and higher elevations, hold most of the low and very low classes (32.09% combined); the very low class alone is marginal (12.24%), which confirms that most of the territory carries at least a moderate predisposition to inundation (Figure 8).

Sensitivity of the zoning to weight perturbations

Table 5 summarizes the sensitivity results. Across the eight perturbation scenarios, the combined extent of the high and very high classes ranges from 40.71% to 43.18%, i.e. a maximum departure of 1.27 percentage points from the reference value of 41.91%, and the rank correlation of the perturbed index with the reference surface never falls below 0.996. The spatial pattern of the zoning - the concentration of the upper classes on the northern coastal plain - is preserved in all scenarios. The map is therefore robust to plausible variations of the expert weights, which addresses the uncertainty introduced by the transfer of the judgment structure from the Berkane setting.

Regional consistency and planning implications

The class structure obtained at Saidia is close to what has been reported for greater Berkane, where 39.23% of the territory fell in the high and very high classes under a comparable eight-factor AHP scheme (Zerhoudi et al., 2026); the slightly larger exposed share found here (41.91%) fits the flatter, more coastal character of the Saidia plain. It departs, on the other hand, from the 31.12% obtained

Table 3. AHP weights and susceptibility direction of the conditioning factors

Rank	Factor	Weight (Wi)	Weight (%)	Hazard direction
1	TWI	0.2801	28.0	Increasing
2	Distance to rivers	0.2017	20.2	Decreasing
3	Slope	0.1790	17.9	Decreasing
4	Elevation	0.1624	16.2	Decreasing
5	Distance to roads	0.0944	9.4	Decreasing
6	Drainage density	0.0499	5.0	Increasing
7	NDVI	0.0325	3.3	Decreasing

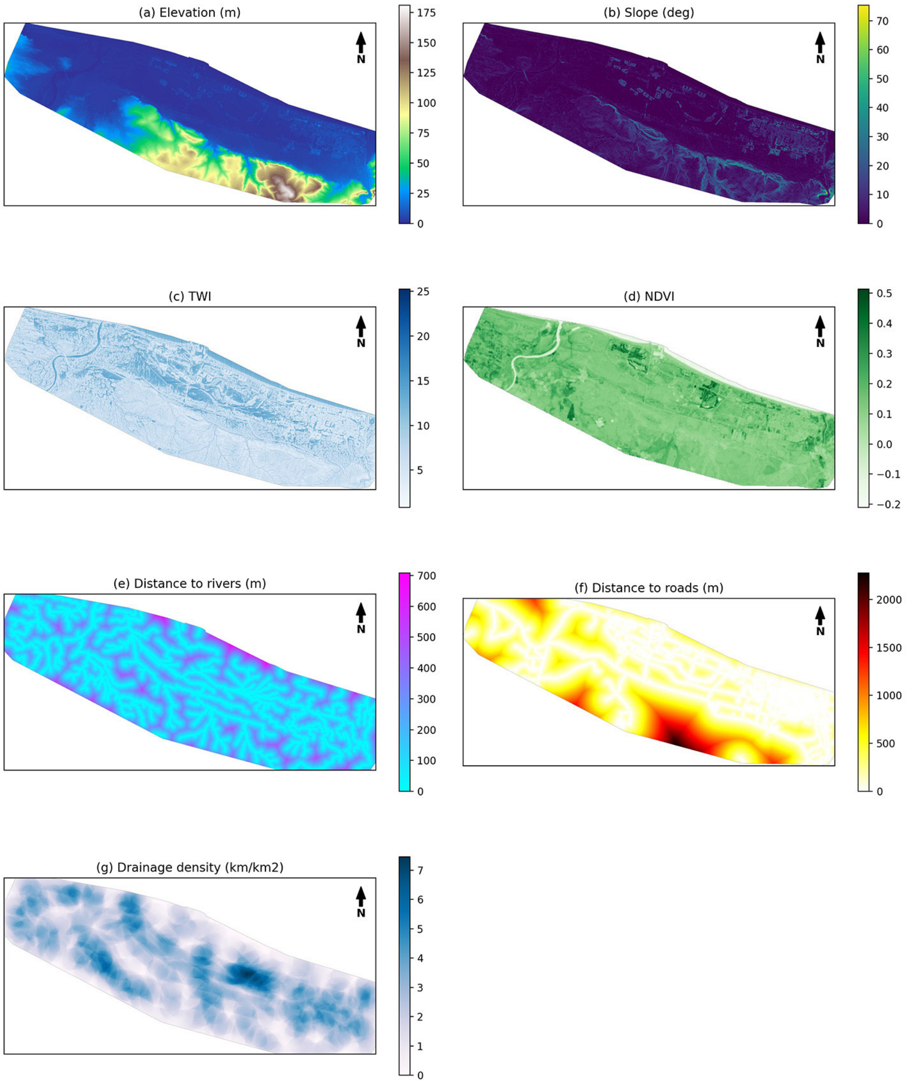

Figure 5. Flood conditioning factors: (a) elevation, (b) slope, (c) TWI, (d) NDVI, (e) distance to rivers, (f) distance to roads, (g) drainage density

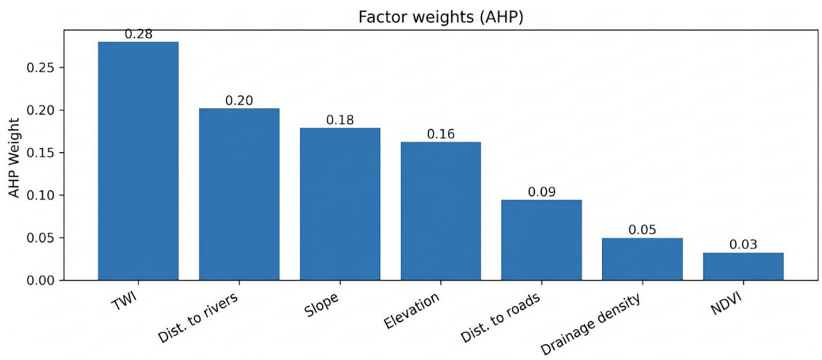

Figure 6. Factor weights derived from the pairwise comparison matrix

with a flood hazard index in the semi-arid Seyad basin (Echogdali et al., 2022), a difference attributable both to the distinct weighting scheme and to the geomorphological contrast between an inland ephemeral-wadi basin and a coastal accumulation plain. The dominant role of river proximity echoes the findings at Driouch, where distance to the channel emerged as the main explanatory factor of flood hazard (El Hadri et al., 2025), and the concentration of the highest classes along an urbanised

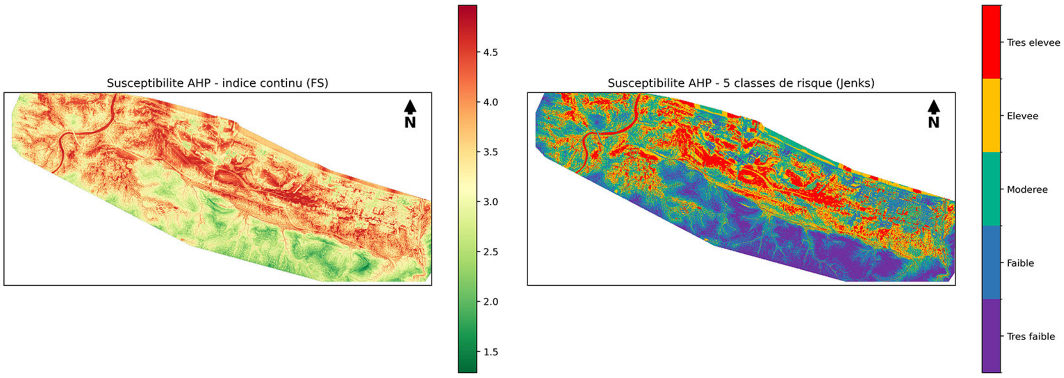

Figure 7. Flood susceptibility over the Saidia coastal area: continuous index (left) and five-class natural-breaks zoning (right)

Table 4. Areal distribution of the susceptibility classes

Class	Susceptibility level	Area (km^2)	Area (%)	Cumulative (%)
1	Very low	8.7	12.24	100.00
2	Low	14.1	19.85	87.76
3	Moderate	18.5	26.01	67.91
4	High	18.6	26.26	41.91
5	Very high	11.1	15.65	15.65

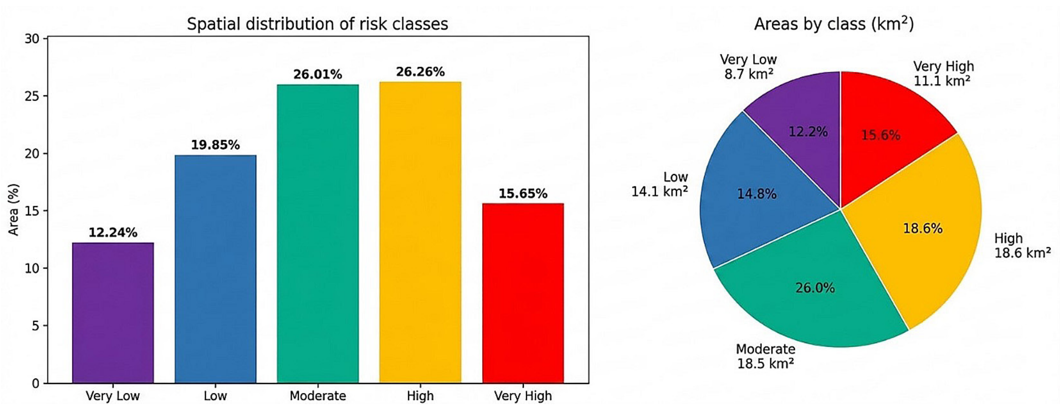

Figure 8. Surface distribution of the susceptibility classes, in percentage (left) and square kilometres (right)

Table 5. One-at-a-time sensitivity of the class-area shares (%) to ±10% and ±20% perturbations of the TWI and distance-to-rivers weights

Scenario	Very low	Low	Moderate	High	Very high	High + Very high	Δ (pts)	Spearman ρ
Reference	12.24	19.85	26.01	26.26	15.65	41.91	0.00	1.000
TWI −20%	12.88	18.41	25.53	27.03	16.15	43.18	+1.27	0.996
TWI −10%	12.57	19.22	26.33	26.61	15.27	41.89	−0.02	0.999
TWI +10%	12.92	20.37	26.01	24.80	15.91	40.71	−1.19	0.999
TWI +20%	13.02	20.51	24.15	25.61	16.72	42.32	+0.42	0.997
Dist. rivers −20%	12.89	19.54	24.63	26.27	16.67	42.94	+1.04	0.997
Dist. rivers −10%	12.81	20.13	25.99	25.14	15.93	41.07	−0.84	0.999
Dist. rivers +10%	12.25	19.21	26.59	26.28	15.67	41.94	+0.04	0.999
Dist. rivers +20%	11.59	18.98	26.28	27.46	15.69	43.15	+1.24	0.997

shoreline mirrors the pattern documented for the coastal reach of Oued Merzeg (Bouchikhi et al., 2025). Together with the Zaio case, where machine-learning hazard maps likewise identified the riverside residential fabric as the critical exposure hotspot (El Baida et al., 2024a), these results point to a regional signature of the lower Moulouya corridor: urban growth pressing against ephemeral channels on low-gradient plains, a trajectory already flagged for the Saidia resort development itself (Aitali et al., 2020).

For planning purposes, the map identifies the northern belt as the priority area for three types of measures: strict control of new construction within the very high class, upgraded stormwater capacity along the road corridors flagged by the distance-to-roads factor, and progressive deployment of nature-based retention and infiltration solutions on the still-unsealed parcels of the high class. Green measures of this kind have proven effective in Mediterranean peri-urban catchments (Ferreira et al., 2020), have been reviewed for urban pluvial settings more broadly (Huang et al., 2020), and have been quantified for the present region under climate-change scenarios (El Baida et al., 2025a); land-use–flood coupling studies further confirm the protective role of vegetated cover (Sun et al., 2018). The continuous FS surface produced by this work lets planners refine class boundaries locally without re-running the full analysis. These measures also underscore the value of integrated watershed management and stormwater-infrastructure planning for reducing hydrological risk in rapidly developing regions (Noor et al., 2025)

Spatial consistency with previous studies

Before comparing the present zoning with the earlier studies of the Saidia area, a methodological caution is in order. Hydraulic models simulate the depth and extent of specific flood scenarios, and inventory-validated hazard maps are benchmarked against observed events; the susceptibility index produced here estimates a time-invariant physical predisposition. Agreement between these products is therefore a spatial consistency assessment - encouraging, but not equivalent to validation, which will only become possible once a local flood inventory is compiled.

The main aim of this study is to characterise flood susceptibility zoning for Saidia City using a GIS-based AHP approach. The results show marked vulnerability in several sectors: the Moulouya riverbank and its surroundings, the urban fabric, and the green spaces of the coastal plain.

Grari (2019) laid the groundwork with a numerical characterisation of the hydrological hazard, using flow–duration–frequency (QdF) curves fitted to the Safsaf gauge and monofrequency synthetic hydrographs; this work captured the macro-scale discharge behaviour of the lower Moulouya and the effect of rapid urban expansion on the protective structures. Building on this, and moving from a macro-hydrological scale to a site-specific physical one, Jouamaa et al. (2024) ran a two-dimensional hydraulic simulation with IBER software, driven by the resulting 50-year hydrograph and built on a high-resolution 1 m digital terrain model (DTM); crossing the water-depth and water-velocity fields showed that the Moulouya River is the dominant driver of flooding and that the urbanised belt is the most vulnerable area. The present paper takes a different route, adding a macro-territorial management dimension through spatial multi-criteria susceptibility mapping and zone classification. Rather than focusing on flow hydrodynamics or localised structural overflows, it maps the predisposition of the whole territory to inundation, offering a planning-grade zoning that complements, and can be checked against, the two physically-based studies that preceded it.

A first-order cross-validation follows directly from this complementarity. For the 50-year event, the peak characteristic daily discharge of the lower Moulouya estimated by Grari (2019) reaches about 2340 m^3/s at Safsaf; propagated through the 1 m IBER model, this discharge produced water depths of 1.33–3.08 m and velocities up to 1.74 m/s over a flooded footprint of 14.46 km^2, of which 7.78 km^2 (53.8%) fell in the high-hazard class (Jouamaa et al., 2024). The spatial pattern of that hydraulically modelled inundation, concentrated along the Moulouya estuarine riverbank, the terminal drainage network, and the low-lying urbanised pockets of the northern coastal plain, coincides closely with the belt classified here as high and very high susceptibility (41.91% of the 71 km^2 domain), which occupies the same near-sea-level, low-gradient sectors. Because the two approaches rest on entirely independent inputs, measured discharge and terrain hydraulics on one side, expert-weighted conditioning factors on the other, their agreement on the location of the critical exposure hotspot amounts to an independent spatial consistency assessment of the susceptibility pattern in the absence of a local flood inventory.

The remaining differences are expected and can be explained: the AHP high and very high area (≈29.7 km²) exceeds the single-event modelled footprint (14.46 km²) because susceptibility expresses a magnitude-independent predisposition rather than the extent of one 50-year flood, and because the AHP domain also captures ephemeral-stream and pluvial contributions that fall outside the strictly fluvial IBER reach. Combined with the class proportions already shown to match the neighbouring Berkane (39.23%) and lower-Moulouya assessments, this convergence is encouraging and increases confidence in the susceptibility pattern, pending the future compilation of a georeferenced flood inventory for formal quantitative validation.

Limitations and perspectives

The main limitation of the present assessment is the lack of a georeferenced inventory of observed flood locations over the study area, which rules out the kind of quantitative validation applied in neighbouring studies through cumulative flood-point statistics (Bouchikhi et al., 2025; Zerhoudi et al., 2026). The judgment matrix, therefore, reflects transferred expertise rather than locally verified judgment. Two extensions serve as potential future prospects: first, validating the mapped results against a historical flood inventory from press archives, satellite imagery, and field surveys, which would allow presence-only validation and support the training of complementary machine learning models (El Baida et al., 2024b; Norallahi and Kaboli, 2021). Second, incorporating coastal drivers such as marine submersion, wave setup, and shallow groundwater is specific to shoreline municipalities and particularly warranted here, since the eastern Mediterranean coast of Morocco ranks among the national segments most vulnerable to sea-level rise (Snoussi et al., 2008) and the local dune system has already been destabilised by recent development (Aitali et al., 2020; Snoussi et al., 2002).

Beyond the absence of a local flood inventory, four sources of uncertainty affect the final map and deserve explicit acknowledgement. The first is the expert judgment encoded in the pairwise matrix: the weights are transferred from a neighbouring setting, and although internally consistent (CR = 0.048), they remain assumptions; this source is the only one amenable to direct quantification here, and the OAT analysis shows that the zoning pattern is robust to plus or minus 10–20% variations of the two dominant weights. The second is factor selection: the seven-factor set characterizes pluvial and fluvial processes only, and the exclusion of marine drivers means that total flood predisposition is bounded from below along the seaward fringe; groundwater conditions are likewise absent. The third is the heterogeneity of native raster resolutions, dominated by the 8 m topographic grid but including a 30 m vegetation index whose low weight (3.3%) bounds its influence. The fourth is the classification scheme: the class boundaries were set by expert judgment rather than by a calibrated hydrological criterion, so the class limits - though not the underlying continuous index, which is distributed with this work – carry a degree of subjectivity. A Monte Carlo propagation of weight uncertainty, sampling the pairwise judgments rather than perturbing the aggregated weights, is identified as the natural next step once a local flood inventory allows the resulting probability envelopes to be benchmarked.

CONCLUSIONS

This paper aims to map pluvial and fluvial flood susceptibility in the coastal lowland city of Saidia using AHP and GIS. The resulting flood susceptibility map classifies 41.91% of the study area as highly to very highly susceptible. These susceptible zones correspond to areas where urbanisation, road corridors, and the Moulouya riverbank coincide with the terminal drainage network. The spatial pattern and class percentages align with recent multi-criteria and machine learning assessments along the lower Moulouya corridor, supporting the transferability of the approach across data-scarce settings of northeastern Morocco and the one-at-a-time sensitivity analysis indicates that the zoning pattern is robust to plus or minus 10–20% variations of the dominant AHP weights. For planning purposes, the northern belt is designated as the priority zone for three targeted measures: strictly controlling new construction in the very high class areas, upgrading stormwater network capacity along critical road corridors, and progressively deploying nature-based retention and infiltration solutions on remaining unpaved parcels of the high class. The zoning is an immediately usable planning document; consolidating it requires building a local flood inventory, hydrodynamic verification, and consideration of the marine flooding component specific to this coastal setting.

REFERENCES

1. Afif, H., Oujidi, M., Chourak, M., Amar, I., Ramdani, S. (2025). Assessment of flood hazards in greater Berkane for the selection of nature-based solutions, Oriental region, Morocco. *Modelling Earth Systems and Environment, 11*(2), 139. https://doi.org/10.1007/s40808-025-02332-z
2. Aichi, A., Ikirri, M., Ait Haddou, M., Quesada-Román, A., Sahoo, S., Singha, C., Sajinkumar, K. S., Abioui, M. (2024). Integrated GIS and analytic hierarchy process for flood risk assessment in the Dades wadi watershed (Central High Atlas, Morocco). *Results in Earth Sciences, 2*, 100019. https://doi.org/10.1016/j.rines.2024.100019
3. Aitali, R., Snoussi, M., Kasmi, S. (2020). Coastal development and risks of flooding in Morocco: The cases of Tahaddart and Saidia coasts. *Journal of African Earth Sciences, 164*, 103771. https://doi.org/10.1016/j.jafrearsci.2020.103771
4. Akay, H. (2021). Flood hazards susceptibility mapping using statistical, fuzzy logic, and MCDM methods. *Soft Computing, 25*(14), 9325–9346. https://doi.org/10.1007/s00500-021-05903-1
5. Armenakis, C., Nirupama, N. (2014). Flood risk mapping for the City of Toronto. *Procedia Economics and Finance, 18*, 320–326. https://doi.org/10.1016/S2212-5671(14)00946-0
6. Asfaha, T. G., Frankl, A., Haile, M., Zenebe, A., Nyssen, J. (2015). Determinants of peak discharge in steep mountain catchments – case of the rift valley escarpment of Northern Ethiopia. *Journal of Hydrology, 529*, 1725–1739. https://doi.org/10.1016/j.jhydrol.2015.08.013
7. Ashfaq, S., Tufail, M., Niaz, A., Muhammad, S., Alzahrani, H., Tariq, A. (2025). Flood susceptibility assessment and mapping using GIS-based analytical hierarchy process and frequency ratio models. *Global and Planetary Change, 251*, 104831. https://doi.org/10.1016/j.gloplacha.2025.104831
8. Bathrellos, G. D., Karymbalis, E., Skilodimou, H. D., Gaki-Papanastassiou, K., Baltas, E. A. (2016). Urban flood hazard assessment in the basin of the Athens metropolitan city, Greece. *Environmental Earth Sciences, 75*(4), 319. https://doi.org/10.1007/s12665-015-5157-1
9. Beven, K. J., Kirkby, M. J. (1979). A physically based, variable contributing area model of basin hydrology. *Hydrological Sciences Bulletin, 24*(1), 43–69. https://doi.org/10.1080/02626667909491834
10. Boughriba, M., Melloul, A., Zarhloule, Y., Ouardi, A. (2006). Extension spatiale de la salinisation des ressources en eau et modèle conceptuel des sources salées dans la plaine des Triffa (Maroc nord-oriental) [Spatial extent of water-resource salinisation and conceptual model of saline springs in the Triffa plain (north-eastern Morocco)]. *Comptes Rendus Geoscience, 338*(11), 768–774. (in French)
11. Bouchikhi, S., Chourak, M., El Baida, M., Boushaba, F. (2025). Multi-criteria decision analysis and hydrodynamic modelling for flood-safe urban planning: Case study of Oued Merzeg, Casablanca (NW Morocco). *Natural Hazards, 121*, 20655–20682. https://doi.org/10.1007/s11069-025-07641-1
12. Chennouf, T., Khattach, D., Milhi, A., Andrieux, P., Keating, P. (2007). Principales lignes structurales du Maroc nord-oriental : apport de la gravimétrie [Main structural lineaments of north-eastern Morocco: Contribution of gravimetry]. *Comptes Rendus Geoscience, 339*(6), 383–395. (in French). https://doi.org/10.1016/j.crte.2007.03.006
13. Deroliya, P., Ghosh, M., Mohanty, M. P., Ghosh, S., Rao, K. H. V. D., Karmakar, S. (2022). A novel flood risk mapping approach with machine learning considering geomorphic and socio-economic vulnerability dimensions. *Science of the Total Environment, 851*, 158002. https://doi.org/10.1016/j.scitotenv.2022.158002
14. Dong, S., Gao, X., Mostafavi, A., Gao, J. (2022). Modest flooding can trigger catastrophic road network collapse due to compound failure. *Communications Earth & Environment, 3*(1), 38. https://doi.org/10.1038/s43247-022-00366-0
15. Dung, N. B., Long, N. Q., Goyal, R., An, D. T., Minh, D. T. (2022). The role of factors affecting flood hazard zoning using analytical hierarchy process: A review. *Earth Systems and Environment, 6*(3), 697–713. https://doi.org/10.1007/s41748-021-00235-4
16. Echogdali, F. Z., Boutaleb, S., Kpan, R. B., Ouchchen, M., Id-Belqas, M., Dadi, B., Ikirri, M., Abioui, M. (2022). Flood hazard and susceptibility assessment in a semi-arid environment: A case study of the Seyad basin, south of Morocco. *Journal of African Earth Sciences, 196*, 104709. https://doi.org/10.1016/j.jafrearsci.2022.104709
17. Eini, M., Kaboli, H. S., Rashidian, M., Hedayat, H. (2020). Hazard and vulnerability in urban flood risk mapping: Machine learning techniques and considering the role of urban districts. *International Journal of Disaster Risk Reduction, 50*, 101687. https://doi.org/10.1016/j.ijdrr.2020.101687
18. El Baida, M., Boushaba, F., Chourak, M., Hosni, M., Sabar, H. (2024a). Flood risk decomposed: Optimised machine learning hazard mapping and multi-criteria vulnerability analysis in the city of Zaio, Morocco. *Journal of African Earth Sciences, 220*, 105431. https://doi.org/10.1016/j.jafrearsci.2024.105431
19. El Baida, M., Hosni, M., Boushaba, F., Chourak, M. (2024b). A systematic literature review on classification machine learning for urban flood hazard mapping. *Water Resources Management, 38*. https://doi.org/10.1007/s11269-024-03940-7

20. El Baida, M., Boushaba, F., Chourak, M., Hosni, M., Sabar, H. (2024c). Classification machine learning models for urban flood hazard mapping: Case study of Zaio, NE Morocco. *Natural Hazards*. https://doi.org/10.1007/s11069-024-06596-z
21. El Baida, M., Chourak, M., Boushaba, F. (2025a). Flood mitigation and water resource preservation: Hydrodynamic and SWMM simulations of nature-based solutions under climate change. *Water Resources Management, 39*(3), 1149–1176. https://doi.org/10.1007/s11269-024-04015-3
22. El Baida, M., Boushaba, F., Chourak, M. (2025b). Drowning overconfidence with uncertainty: Mitigating deep learning overconfidence in flood depth super-resolution through maximum entropy regularisation. *Stochastic Environmental Research and Risk Assessment, 39*, 1159–1177. https://doi.org/10.1007/s00477-025-02917-1
23. El Hadri, L., Boushaba, F., Chourak, M., El Baida, M. (2025). Mapping flood hazard in Driouch region (north-eastern Morocco) using AHP and numerical approaches. *Journal of African Earth Sciences, 231*, 105776. https://doi.org/10.1016/j.jafrearsci.2025.105776
24. El Idrysy, E. H., De Smedt, F. (2006). Modelling groundwater flow of the Trifa aquifer, Morocco. *Hydrogeology Journal, 14*, 1265–1276. https://doi.org/10.1007/s10040-006-0080-x
25. Elsadek, W. M., Wahba, M., Al-Arifi, N., Kanae, S., El-Rawy, M. (2024). Scrutinising the performance of GIS-based analytical hierarchical process approach and frequency ratio model in flood prediction – case study of Kakegawa, Japan. *Ain Shams Engineering Journal, 15*(2), 102453. https://doi.org/10.1016/j.asej.2023.102453
26. Fan, Y., Clark, M., Lawrence, D. M., Swenson, S., Band, L. E., Brantley, S. L., et al. (2019). Hillslope hydrology in global change research and Earth system modelling. *Water Resources Research, 55*(2), 1737–1772. https://doi.org/10.1029/2018WR023903
27. Ferreira, C. S. S., Mourato, S., Kasanin-Grubin, M., Ferreira, A. J. D., Destouni, G., Kalantari, Z. (2020). Effectiveness of nature-based solutions in mitigating flood hazard in a Mediterranean peri-urban catchment. *Water, 12*(10), 2893. https://doi.org/10.3390/w12102893
28. Fetouani, S., Sbaa, M., Vanclooster, M., Bendra, B. (2008). Assessing groundwater quality in the irrigated plain of Triffa (north-east Morocco). *Agricultural Water Management, 95*(2), 133–142.
29. Frimpong, R. A., Adjei-Yeboah, S., Bohat, N., Sunkari, E. D., Hemans, I. A., El Afandi, G. (2026). Assessment of flood susceptibility in the Oti region of Ghana utilising GIS-based analytical hierarchy process and frequency ratio model. *Journal of African Earth Sciences, 240*, 106148. https://doi.org/10.1016/j.jafrearsci.2026.106148
30. Gnann, S., Baldwin, J. W., Cuthbert, M. O., Gleeson, T., Schwanghart, W., Wagener, T. (2025). The influence of topography on the global terrestrial water cycle. *Reviews of Geophysics, 63*(1), e2023RG000810. https://doi.org/10.1029/2023RG000810
31. Grari, A. (2019). Caractérisation numérique de l'aléa du risque d'inondations sur la ville de Saïdia [Numerical characterisation of flood-risk hazard for the city of Saidia] [Doctoral thesis, Université Mohammed Premier, Faculté des Sciences Oujda]. (in French)
32. Hasanuzzaman, M., Shit, P. K., Bera, B., Islam, A. (2023). Characterising recurrent flood hazards in the Himalayan foothill region through data-driven modelling. *Advances in Space Research, 71*(12), 5311–5326. https://doi.org/10.1016/j.asr.2023.02.028
33. Huang, Y., Tian, Z., Ke, Q., Liu, J., Irannezhad, M., Fan, D., Hou, M., Sun, L. (2020). Nature-based solutions for urban pluvial flood risk management. *WIREs Water, 7*(3), e1421. https://doi.org/10.1002/wat2.1421
34. Jouamaa, A., Chourak, M., Boushaba, F., Sabar, H., Chaaraoui, A. (2024). Two-dimensional flooding model using IBER software case study: Saidia City, northeast of Morocco. *E3S Web of Conferences, 502*, 03011.
35. Kantoush, S. A., Sabre, M., Abdel-Fattah, M., Sumi, T. (2022). Integrated strategies for the management of wadi flash floods in the Middle East and North Africa (MENA) arid zones: The ISFF project. In *Wadi flash floods: Challenges and advanced approaches for disaster risk reduction* (pp. 3–34). Springer. https://doi.org/10.1007/978-981-16-2904-4_1
36. Kelleher, C., McPhillips, L. (2020). Exploring the application of topographic indices in urban areas as indicators of pluvial flooding locations. *Hydrological Processes, 34*(3), 780–794. https://doi.org/10.1002/hyp.13628
37. Loudyi, D., Kantoush, S. A. (2020). Flood risk management in the Middle East and North Africa (MENA) region. *Urban Water Journal, 17*(5), 379–380. https://doi.org/10.1080/1573062X.2020.1777754
38. Maranzoni, A., D'Oria, M., Rizzo, C. (2023). Quantitative flood hazard assessment methods: A review. *Journal of Flood Risk Management, 16*(1), e12855. https://doi.org/10.1111/jfr3.12855
39. Mudashiru, R. B., Sabtu, N., Abustan, I. (2021a). Quantitative and semi-quantitative methods in flood hazard/susceptibility mapping: A review. *Arabian Journal of Geosciences, 14*(11), 941. https://doi.org/10.1007/s12517-021-07263-4
40. Mudashiru, R. B., Sabtu, N., Abustan, I., Balogun, W. (2021b). Flood hazard mapping methods: A review. *Journal of Hydrology, 603*, 126846. https://doi.org/10.1016/j.jhydrol.2021.126846

41. Nachappa, T. G., Ghorbanzadeh, O., Gholamnia, K., Blaschke, T. (2020). Multi-hazard exposure mapping using machine learning for the State of Salzburg, Austria. *Remote Sensing, 12*(17), 2757. https://doi.org/10.3390/rs12172757
42. Norallahi, M., Kaboli, H. S. (2021). Urban flood hazard mapping using machine learning models: GARP, RF, MaxEnt and NB. *Natural Hazards, 106*(1), 119–137. https://doi.org/10.1007/s11069-020-04453-3
43. Noor, S., Salman, A., Alam, F., Bo, D., Ali, B., Khan, G. D., Shahid, R. (2025). Environmental assessment of the Auxiliary Kandar Dam and its influence on the lifespan extension of the main reservoir: Evidence from Kohat, Pakistan. *Trends in Ecological and Indoor Environmental Engineering, 3*(4), 12–22.
44. Odiana, S., Godwin, O. G., Okoduwa, A. K. (2026). Integrating long-term climate trend analysis and household socioeconomic vulnerability to assess climate stress in the Niger Delta floodplain (Ughelli, Nigeria). *Trends in Ecological and Indoor Environmental Engineering, 4*(2), 12–21.
45. Özay, B., Orhan, O. (2023). Flood susceptibility mapping by best–worst and logistic regression methods in Mersin, Turkey. *Environmental Science and Pollution Research, 30*(15), 45151–45170. https://doi.org/10.1007/s11356-023-25423-9
46. Pourali, S. H., Arrowsmith, C., Chrisman, N., Matkan, A. A., Mitchell, D. (2016). Topography wetness index application in flood-risk-based land use planning. *Applied Spatial Analysis and Policy, 9*(1), 39–54. https://doi.org/10.1007/s12061-014-9130-2
47. Ramkar, P., Yadav, S. M. (2021). Flood risk index in data-scarce river basins using the AHP and GIS approach. *Natural Hazards, 109*(1), 1119–1140. https://doi.org/10.1007/s11069-021-04871-x
48. Saaty, T. L. (1977). A scaling method for priorities in hierarchical structures. *Journal of Mathematical Psychology, 15*(3), 234–281. https://doi.org/10.1016/0022-2496(77)90033-5
49. Sardinha, J., Carneiro, J. F., Zarhloule, Y., Barkaoui, A., Correia, A., Boughriba, M., Rimi, A., El Houadi, B. (2012). Structural and hydrogeological features of a Lias carbonate aquifer in the Triffa plain, NE Morocco. *Journal of African Earth Sciences, 73–74*, 24–32. https://doi.org/10.1016/j.jafrearsci.2012.06.006
50. Shikhteymour, S. R., Borji, M., Bagheri-Gavkosh, M., Azimi, E., Collins, T. W. (2023). A novel approach for assessing flood risk with machine learning and multi-criteria decision-making methods. *Applied Geography, 158*, 103035. https://doi.org/10.1016/j.apgeog.2023.103035
51. Skilodimou, H. D., Bathrellos, G. D., Pappa, M.-I., Youssef, A. M., Kontakiotis, G., Karymbalis, E. (2025). Assessing flood hazard mapping using AHP and GIS in a tectonically active region. *Zeitschrift für Geomorphologie, 64*(3–4), 275–288. https://doi.org/10.1127/zfg/2024/0804
52. Snoussi, M., Haïda, S., Imassi, S. (2002). Effects of the construction of dams on the water and sediment fluxes of the Moulouya and the Sebou Rivers, Morocco. *Regional Environmental Change, 3*(1), 5–12. https://doi.org/10.1007/s10113-001-0035-7
53. Snoussi, M., Ouchani, T., Niazi, S. (2008). Vulnerability assessment of the impact of sea-level rise and flooding on the Moroccan coast: The case of the Mediterranean eastern zone. *Estuarine, Coastal and Shelf Science, 77*(2), 206–213. https://doi.org/10.1016/j.ecss.2007.09.024
54. Sun, D., Yang, H., Guan, D., Yang, M., Wu, J., Yuan, F., Jin, C., Wang, A., Zhang, Y. (2018). The effects of land use change on soil infiltration capacity in China: A meta-analysis. *Science of the Total Environment, 626*, 1394–1401. https://doi.org/10.1016/j.scitotenv.2018.01.104
55. Tehrany, M. S., Pradhan, B., Mansor, S., Ahmad, N. (2015). Flood susceptibility assessment using a GIS-based support vector machine model with different kernel types. *Catena, 125*, 91–101. https://doi.org/10.1016/j.catena.2014.10.017
56. Teng, J., Jakeman, A. J., Vaze, J., Croke, B. F. W., Dutta, D., Kim, S. (2017). Flood inundation modelling: A review of methods, recent advances and uncertainty analysis. *Environmental Modelling & Software, 90*, 201–216. https://doi.org/10.1016/j.envsoft.2017.01.006
57. Tramblay, Y., Badi, W., Driouech, F., El Adlouni, S., Neppel, L., Servat, E. (2012). Climate change impacts on extreme precipitation in Morocco. *Global and Planetary Change, 82–83*, 104–114. https://doi.org/10.1016/j.gloplacha.2011.12.002
58. Tramblay, Y., Villarini, G., El Khalki, E. M., Gründemann, G., Hughes, D. (2021). Evaluation of the drivers responsible for flooding in Africa. *Water Resources Research, 57*(6), e2021WR029595. https://doi.org/10.1029/2021WR029595
59. Tramblay, Y., Villarini, G., Saidi, M. E., Massari, C., Stein, L. (2022). Classification of flood-generating processes in Africa. *Scientific Reports, 12*(1), 18920. https://doi.org/10.1038/s41598-022-23725-5
60. Vu, H. C., To, T. N., Le, H. (2024). Impacts of the road on flood inundation in the Tra Khuc–Ve River basin, Vietnam. *Water Policy, 26*(12), 1261–1282. https://doi.org/10.2166/wp.2024.313
61. Zerhoudi, I., Chourak, M., El Baida, M., Boushaba, F., Louhibi, S. (2026). Multi-criteria decision making and presence-only maximum entropy modelling for flood hazard assessment in Greater Berkane. *Journal of African Earth Sciences, 240*, 106179. https://doi.org/10.1016/j.jafrearsci.2026.106179